Electronic Supplementary Material (ESI) for Chemical Science.
This journal is © The Royal Society of Chemistry 2019

Electronic Supplementary Information (ESI) for

Quantitative insights into charge-separated states from one- and two-pulse laser experiments relevant for artificial photosynthesis

Svenja Neumann, Christoph Kerzig* and Oliver S. Wenger*

Contents

1 General experimental details S1

1.1 Materials S1

1.2 Equipment and methods S2

1.3 Laser setup and quantitative laser flash photolysis S2

2 Energies of charge-separated states S4

3 Quantum-mechanical calculations S6

4 Additional laser flash photolysis data S7

4.1 Single-pulse experiments S7

4.2 Two-pulse experiments S9

5 Supplementary references S10

1 General experimental details

1.1 Materials

The compounds under study, except rutheniumtris(bipyridine) dichloride hexahydrate, have been prepared and characterized according to our previously reported procedure.[1] Rutheniumtris(bipyridine) dichloride hexahydrate (99.95%, Aldrich), tetrabutylammonium hexafluorophosphate ($TBAPF_6$, for electrochemical analysis, ≥99.0%, Aldrich) and copper(II) perchlorate hexahydrate (99.999% (metals basis), Alfa Aesar) were purchased from

commercial suppliers and used as received. The solvent for experiments with rutheniumtris(bipyridine) ($[Ru(bpy)_3]^{2+}$) dichloride hexahydrate was ultrapure Millipore MilliQ water (specific resistance, 18.2 MΩ cm), whereas commercially available CH_3CN (anhydrous 99.8 %, Aldrich) was used for optical spectroscopy and irradiation experiments of the compounds under study. Unless stated otherwise, the solutions prepared for laser flash photolysis experiments were deoxygenated with argon (4.8, PanGas) using several cycles of the freeze–pump–thaw technique.

1.2 Equipment and methods

All cyclic voltammetry measurements were performed in dry and deoxygenated CH_3CN with $TBAPF_6$ (0.1 M) as electrolyte. A scan rate of 0.1 V/s was applied. An SCE was used as reference, a glassy carbon disk electrode served as working electrode and a silver wire was used as counter electrode. To apply and control the voltage, a Versastat3-200 potentiostat from Princeton Applied Research was used. Steady-state optical absorption spectroscopy was performed on a Cary 5000 instrument from Varian with quartz cuvettes of 1 cm pathlength. If deoxygenated conditions were applied, home-built quartz cuvettes with 1 cm pathlengths were used. UV-Vis transient absorption and emission measurements, together with kinetic studies, were carried out on an LP920-KS instrument from Edinburgh Instruments. A more precise description of the used setup can be found in the next subsection. All spectroscopic experiments of this study were carried out at 293 K.

1.3 Laser setup and quantitative laser flash photolysis

An LP920-KS apparatus from Edinburgh Instruments was used to investigate transient species. Excitation of our Ir-containing compounds was carried out by a Quantel Brilliant laser equipped with an OPO from Opotek using excitation wavelengths between 410 und 470 nm. A second Nd:YAG laser (Quantel Brilliant b, *ca.* 10 ns pulse width) operating at 532 nm was used to investigate the photoinduced recombination of the CSSs. All quantitative laser experiments were accompanied by actinometry experiments on the reference compound $[Ru(bpy)_3]^{2+}$ (see next page for details). Synchronization of the two lasers and the detection system was achieved as described previously.[2] The excitation intensities of both lasers were varied by the Q-switch delays and measured with a pyroelectric detector from Ophir immediately before starting the experiments. Control measurements established the laser output stability during each series of experiments.
The beams of both lasers were sent through beam expanders (GBE02-A or GBE05-A, both from Thorlabs) to bring their diameters to either ~1.4 cm (blue laser; maximum laser intensity per area, 13 mJ cm^{-2}) or ~1.2 cm (green laser; maximum laser intensity per area, 125 mJ cm^{-2}). The beam expansion ensured completely homogeneous laser excitation in the whole detection volume (about 1.2 cm^3). The lasers were carefully adjusted before starting the measurements, especially for two-pulse experiments, in which the beam overlap is important. Detection of transient absorption spectra occurred on an iCCD camera from

Andor (with time-integration over 200 ns), while kinetic traces at a single wavelength were recorded using a photomultiplier tube.

We attribute the observed CSS lifetime increase of **TAA-ph$_1$-Ir-ph$_1$-AQ** from ~1.0 μs[1] to ~1.2 μs (this study) to the widely differing local CSS concentrations in the detection volume after the laser pulses. The area-normalized laser intensities in our recent study (~120 mJ cm^{-2}, without beam expansion)[1] were about one order of magnitude higher than in the experiments presented in this paper (<13 mJ cm^{-2}, with beam expansion). The microsecond CSS lifetime in combination with high local CSS concentrations could enable self-quenching reactions, and thus account for our observations. A kinetic simulation with simultaneous first-order CSS decay (natural lifetime, 1.2 microseconds) and diffusion-controlled[3] CSS self-quenching could indeed reproduce the observed ~17% lifetime reduction, when we assume a CSS concentration as high as ~13 μM in the pump volume right after high-intensity laser excitation. That reasoning is in line with the unchanged lifetime results for **TAA-ph$_2$-Ir-ph$_2$-AQ**, whose short lifetime (<100 ns) does not permit bimolecular reactions between two excited molecules. The slight lifetime increase of **TAA-ph$_1$-Ir-ph$_1$-AQ** does not affect the conclusions drawn in ref. [1].
Using the expanded blue laser beam, we observed a significantly improved photostability of all Ir-containing compounds. Without beam expander, fresh (*i.e.*, unirradiated) solutions were used for every experiment since minor changes in the UV-Vis spectra (indicating photodegradation) were detected after about 200 pulses on the same solution.[1] However, the solutions irradiated with beam expander between laser and cuvettes did not show any detectable changes even after more than 1000 laser flashes.

Quantitative one- and two-pulse laser flash photolysis measurements were carried out using chemical actinometry[4] with the excitation of $[Ru(bpy)_3]^{2+}$ into its triplet state (quantum yield, 1.0)[5] as widely accepted reference reaction. Aqueous $[Ru(bpy)_3]^{2+}$ solutions were used for the following reasons: (i) The molar absorption coefficient for the $[Ru(bpy)_3]^{2+}$ ground state bleach is well-established in water ($\Delta\varepsilon_{455} = -10100$ M^{-1} cm^{-1})[6–9]. (ii) ^{3}MLCT formation is the only detectable photochemical process upon visible light absorption by $[Ru(bpy)_3]^{2+}$ in water;[6,10] moreover, this actinometry system is even reliable at moderate laser pulse intensities (up to ~30 mJ cm^{-2}) under UVA excitation conditions, which in principle allow the biphotonic ionization of $[Ru(bpy)_3]^{2+}$.[7,11,12] (iii) Since the refractive indices of water and acetonitrile (solvent for the Ir-containing compounds) differ by less than 1%,[3] corrections of the transient absorption data are unnecessary. (iv) Oxygen removal from the aqueous $[Ru(bpy)_3]^{2+}$ solutions is not required, because $^3[Ru(bpy)_3]^{2+}$ lives long enough in air-saturated water (about 400 ns) for a sensitive detection, and $[Ru(bpy)_3]^{2+}$ is not prone to fast photooxidation under these conditions.[8]

The knowledge of the calibrated absorption spectrum of the respective CSS is a basic requirement for all quantitative laser investigations on **TAA-ph$_1$-Ir-ph$_1$-AQ** and **TAA-ph$_2$-Ir-ph$_2$-AQ**. Guided by successful molar absorption coefficient determinations of triarylamines

by chemical oxidation experiments,[13] we first tried to quantitatively oxidize our triads with copper(II) perchlorate, and monitored the spectra of their triarylamine radical cations using steady-state UV-Vis spectroscopy. However, the molar absorption coefficients of $TAA^{\bullet+}$ so obtained depend strongly on the rate of the redox titration and are systematically too low (< 15000 M^{-1} cm^{-1} at the $TAA^{\bullet+}$ absorption maximum in the red), as a comparison with typical literature values shows.[13–15] We attribute these observations to undesired side reactions, which have already been reported for triarylamine radical cations lacking of additional stabilization through methoxy substituents.[16]

Another possibility for calibrating the CSS absorption spectra is provided by the anthraquinone radical anion ($AQ^{\bullet-}$) absorption bands. In contrast to the $TAA^{\bullet+}$ absorptions of the triads in the red region of the visible spectrum, whose maxima differ by about 20 nm, shape and position of the dominant $AQ^{\bullet-}$ absorption at ~560 nm are identical in both triads, as spectroelectrochemical measurements[1] and transient absorption studies (Fig. S5 of the ESI) clearly demonstrate. It seems natural to assume that this species contributes in the same way to the CSSs of the Ir triads under study. Assuming a negligible effect of the adjacent *p*-xylene bridge, we took the mean extinction coefficient at maximum of two previous $AQ^{\bullet-}$ studies in organic solvents, 15100 M^{-1} cm^{-1}.[17,18] With that value and the (uncalibrated) spectroelectrochemical signatures of both $AQ^{\bullet-}$ and $TAA^{\bullet+}$ in the CSS of the respective triad ($TAA^{\bullet+}$ still absorbs at the $AQ^{\bullet-}$ maximum, which necessitated a spectral separation),[1] the calibrated CSS absorption spectra were obtained. The molar absorption coefficients at maximum intensity so obtained are 29900 M^{-1} cm^{-1} (720 nm) and 24700 M^{-1} cm^{-1} (700 nm) for **TAA-ph$_1$-Ir-ph$_1$-AQ** and **TAA-ph$_2$-Ir-ph$_2$-AQ**, respectively. These values were used to convert the CSS transient absorption signals into transient CSS concentrations.

The molar absorption coefficients of both CSSs at the wavelength of the second laser, 532 nm, are essential for quantifying the efficiency of second-pulse induced processes. The pertinent coefficients are 15500 M^{-1} cm^{-1} (**TAA-ph$_1$-Ir-ph$_1$-AQ**) and 15800 M^{-1} cm^{-1} (**TAA-ph$_2$-Ir-ph$_2$-AQ**). The anthraquinone radical anion is the dominant absorbing species at this wavelength. The $AQ^{\bullet-}$ contributions to the overall extinction coefficients at 532 nm are 68% (**TAA-ph$_1$-Ir-ph$_1$-AQ**) and 66% (**TAA-ph$_2$-Ir-ph$_2$-AQ**).

2 Energies of charge-separated states

The energy of the charge-separated state (CSS) can be derived from the redox potentials of $AQ^{\bullet-}$ and $TAA^{\bullet+}$ in the respective triad since the stored energy (E_{CSS}) is equivalent to the driving force ($-\Delta G_{CR}^0$) of the thermal charge recombination process of the photoexcited triad. The redox potentials of the individual components of the triads were determined by cyclic voltammetry (Fig. S1 and Fig. 1b of the main paper). Experimental details are given in Section 1.2 of the ESI as well as in the caption of Fig. S1.

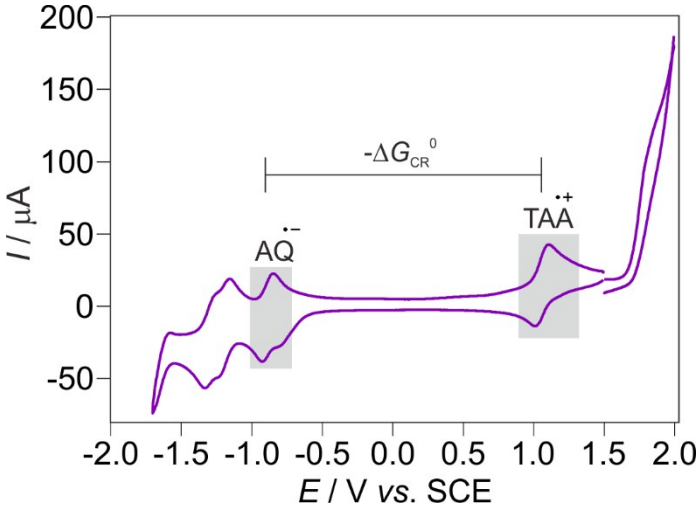

Fig. S1: Cyclic voltammogram of **TAA-ph$_2$-Ir-ph$_2$-AQ** in deoxygenated CH_3CN with $TBAPF_6$ (0.1 M) as an electrolyte. A scan rate of 0.1 V/s was applied. For further explanations, see text.

In analogy to the shorter triad **TAA-ph$_1$-Ir-ph$_1$-AQ** (main part of the paper, Fig. 1b), the one-electron oxidations of the TAA donor unit and of the iridium moiety are observed when oxidative sweeps are performed with **TAA-ph$_2$-Ir-ph$_2$-AQ** (Fig. S1). Likewise, a first (one-electron) reduction of the AQ acceptor, which is followed by the reduction of the bipyridine unit, is observed when performing reductive cyclic voltammetry sweeps. Afterwards, the second reduction of the AQ unit to the quinone dianion occurs before the dF(CF_3)ppy ligands are each reduced by one electron.

Table S1. Redox potentials (in V *vs.* SCE) extracted from Fig. 1b of the main part of the paper and Fig. S1.

Redox potentials	TAA-ph$_1$-Ir-ph$_1$-AQ	TAA-ph$_2$-Ir-ph$_2$-AQ
E^0(dF(CF_3)ppy$^{-/2-}$)[a]	-1.88	-1.88
E^0(dF(CF_3)ppy$^{-/2-}$)[a]	-1.65	-1.62
E^0(AQ$^{-/2-}$)	-1.30	-1.30
E^0(bpy$^{0/-}$)	-1.19	-1.19
E^0(AQ$^{0/-}$)	-0.86	-0.89
E^0(TAA$^{+/0}$)	1.11	1.06
E^0(Ir$^{IV/III}$)	1.78	1.75

[a] Not shown in Fig. 1b of the main part of the paper and Fig. S1 for clarity of the voltammograms. The values were measured under identical conditions as described above.

The driving force for thermal charge recombination corresponds to the negative reaction free energy (ΔG_{CR}^0) for electron transfer from the reduced acceptor ($AQ^{\bullet-}$) to the oxidized donor ($TAA^{\bullet+}$) in the triads under study. Estimations of ΔG_{CR}^0 were performed using equation S1[19] and the reported redox potentials in Table S1. e is the elemental charge, ε_0 is the

vacuum permittivity, and ε_S is the dielectric constant of the solvent (35.9 for CH_3CN)[20]. The used center-to-center distances (r_{DA}) are 22.0 Å for **TAA-ph$_1$-Ir-ph$_1$-AQ** and 30.6 Å for **TAA-ph$_2$-Ir-ph$_2$-AQ**.[1] r_{DA} corresponds to the distance between the N-atom of the TAA donor and the centroid of the anthraquinone acceptor unit. Calculated values for the driving force are given in Table S2.

$$\Delta G_{CR}{}^{0} = e \cdot \left[E^{0}(AQ^{0/-}) - E^{0}(TAA^{+/0})\right] - \frac{e^{2}}{4\pi\varepsilon_{0}\varepsilon_{s}r_{DA}} \qquad \text{(eq S1)}$$

Table S2. Estimated driving forces ($-\Delta G_{CR}{}^{0}$) for thermal charge recombination on the basis of the redox potentials in Table S1. $-\Delta G_{CR}{}^{0}$ corresponds to the energy stored in the CSS of the respective triad.

Triad	$-\Delta G_{CR}{}^{0}$ [eV]
TAA-ph$_1$-Ir-ph$_1$-AQ	1.99
TAA-ph$_2$-Ir-ph$_2$-AQ	1.96

3 Quantum-mechanical calculations

Guided by energetic considerations, we recently explained the additional shoulder in the UV-Vis absorption spectrum of **TAA-ph$_1$-Ir-ph$_1$-AQ** as compared to **TAA-ph$_2$-Ir-ph$_2$-AQ** by an intraligand charge transfer (CT) from the triarylamine donor to the bipyridine moiety.[1] In order to provide further support for that hypothesis, DFT calculations were carried out with the Gaussian 09 package[21] using the B3LYP functional and the 6-31+G(d,p) basis set. Rather than trying to optimize the full heavy-metal containing complexes with a smaller basis set, we performed calculations on the ligands with simplified structures (*i.e.*, without anthraquinone parts and Ir{dF(CF_3)ppy}$_2$ fragments).

The optimized geometries of the two model compounds are displayed in Fig. S2. These optimizations were accompanied by frequency analyses, which did not show negative vibrational frequencies indicating convergence on minimum structures. Based on the optimized structures, population analyses were carried out to obtain the orbitals displayed in Fig. S2. The HOMOs of both ligand fragments are TAA-localized, whereas the LUMOs are mainly centered on the bipyridine moiety. Additional time-dependent(TD)-DFT calculations revealed substantially different properties of the lowest energy transition in both structures; for the shorter structure with one *p*-xylene spacer between TAA nitrogen atom and bipyridine, we found a high oscillator strength being in line with the significant overlap integral of the frontier orbitals (Fig. S2, upper row), however, as a result of the additional xylene unit, that transition is completely forbidden in the longer structure (Fig. S2, lower row).

Despite the usage of strongly simplified structures for our calculations, the results summarized in Fig. S2 clearly substantiate the recent explanation of the additional

absorption band in the shorter triad **TAA-ph$_1$-Ir-ph$_1$-AQ** by a CT between triarylamine and bipyridine.

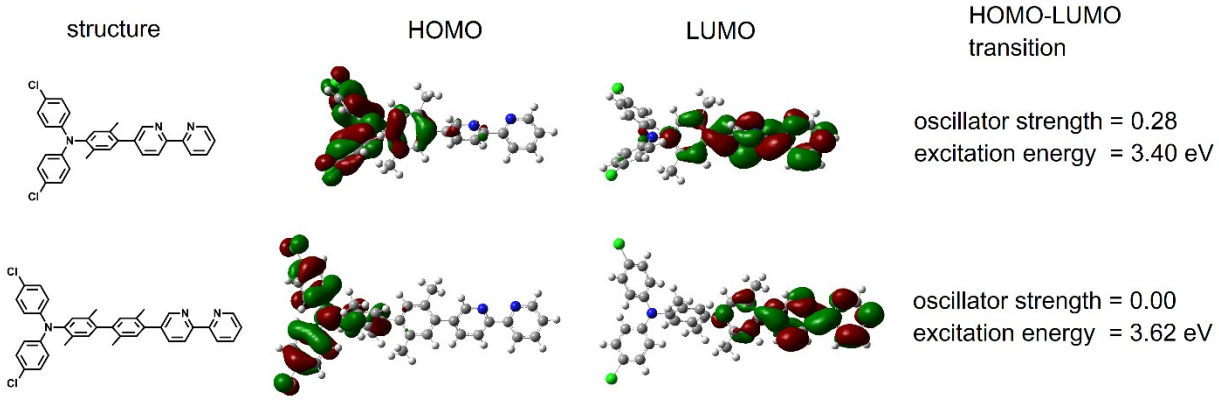

Fig. S2: Chemical structure of the two model compounds, their DTF-optimized structures (computed at the B3LYP/6-31+G(d,p) level of theory) together with the corresponding frontier orbitals, and properties of the HOMO-LUMO transitions. For details, see text.

4 Additional laser flash photolysis data

4.1 Single-pulse experiments

Additional single-pulse experiments on the reference compound **Ir-Ref** are shown in Fig. S3. The transient absorption spectrum following 410 nm laser excitation is practically identical to that presented in our recent study.[1] However, owing to the improved excitation homogeneity in the detection volume when using the beam expander (compare, Section 1.3 of the ESI) and consequently the optimized spatial overlap between pump and probe beams, the signal-to-noise ratio is significantly higher in the present study. Moreover, the emission spectrum of **Ir-Ref** at room temperature (293 K) was measured (upper inset of Fig. S3) to identify the emission maximum, at which additional kinetic emission traces were recorded for **Ir-Ref** and both triads (see, Fig. S4).

As we found by kinetic measurements (lower inset of Fig. S3), both the transient absorption (detection at 570 nm) and emission (detection at 530 nm) signal decays are almost perfectly monoexponential with identical lifetimes, 14.1 μs. It is worth mentioning that the so-obtained excited-state lifetime of **Ir-Ref** is longer by a factor of six compared to those of structurally similar complexes with simple bipyridine or di-*tert*-butyl-bipyridine diimine ligands under identical conditions.[22,23] Given that the latter complex, $[Ir\{dF(CF_3)ppy\}_2(dtbpy)]PF_6$, is a commercial and widely-used photoredox catalyst,[24] the much longer lifetime of excited **Ir-Ref** (together with practically identical (photo)redox properties as $[Ir\{dF(CF_3)ppy\}_2(dtbpy)]^+$)[1] might be beneficial for photochemical applications.

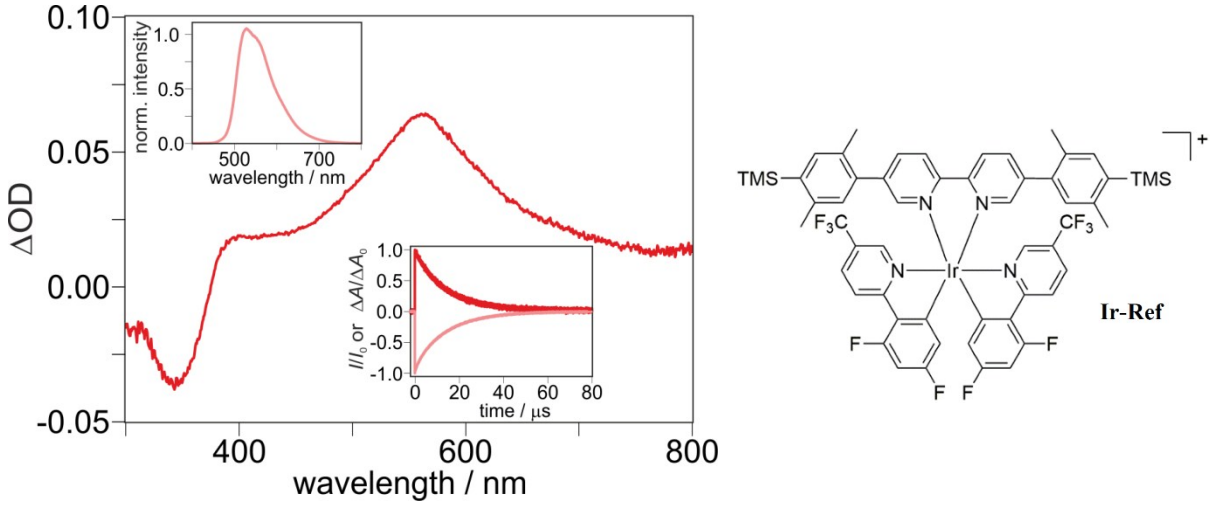

Fig. S3: Excited-state properties of **Ir-Ref**, whose structure is shown on the right. Main plot, transient absorption spectrum of **Ir-Ref** (20 μM in dry and deoxygenated CH_3CN) following laser excitation at 410 nm (8 mJ). The spectrum was recorded by time-averaging over a period of 200 ns immediately after excitation. Upper inset, emission spectrum of **Ir-Ref** under the conditions as in the main plot, but time-averaged over 10 μs. Lower inset, kinetic absorption and emission data with the same color code as in the corresponding spectra.

Comparative kinetic emission traces for the three Ir-containing compounds under identical excitation and detection conditions are shown in Fig. S4. The MLCT emission of the triads is almost instantaneously quenched indicating that the MLCT lifetime is significantly shorter than the laser pulse duration (~10 ns). A more detailed discussion of these measurements can be found in Section 2.3 of the main paper.

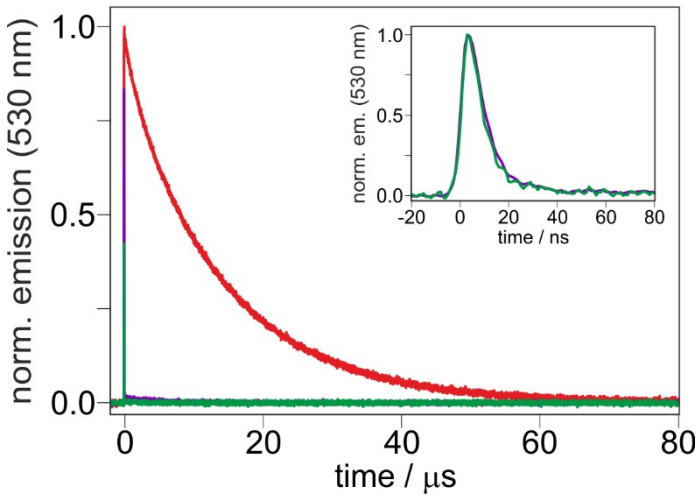

Fig. S4: Kinetic emission traces of **TAA-ph$_1$-Ir-ph$_1$-AQ** (green), **TAA-ph$_2$-Ir-ph$_2$-AQ** (violet) and **Ir-Ref** (red) after 410 nm excitation (8 mJ laser pulses of ~10 ns duration) of Ar-saturated CH_3CN solutions with an OD of ~0.1 at the excitation wavelength recorded at the maximum of the **Ir-Ref** MLCT emission (530 nm). The inset shows the emission traces of the triads on a nanosecond timescale. For further explanation see text and main part of the paper.

The excitation wavelength dependent transient absorption spectra collected in Fig. S5 prove that the CSSs are the only detectable intermediates upon visible light excitation of our triads (see also Section 2.3 of the main paper; for clarity, only three spectra for each triad are shown).

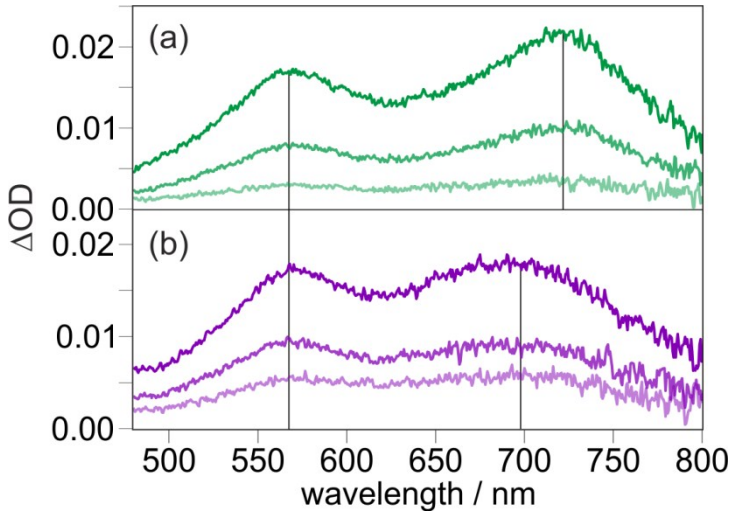

Fig. S5: Transient absorption spectra (time-integrated over 200 ns immediately following excitation) of **TAA-ph$_1$-Ir-ph$_1$-AQ** (a) and **TAA-ph$_2$-Ir-ph$_2$-AQ** (b) recorded at different excitation wavelengths (**TAA-ph$_1$-Ir-ph$_1$-AQ**: 410 nm, 440 nm and 470 nm; **TAA-ph$_2$-Ir-ph$_2$-AQ**: 410 nm, 433 nm and 450 nm) in deoxygenated CH_3CN at 293 K. Spectral range chosen such that the dominant $AQ^{\bullet-}$ (~570 nm) and $TAA^{\bullet+}$ (red edge of the visible spectrum) absorption bands are displayed.

4.2 Two-pulse experiments

The same data set as in Fig. 5a of the main paper is displayed in Fig. S6. The logarithmic representation used in Fig. S6, however, facilitates illustrating the first-order recombination kinetics of the **TAA-ph$_1$-Ir-ph$_1$-AQ** CSS.

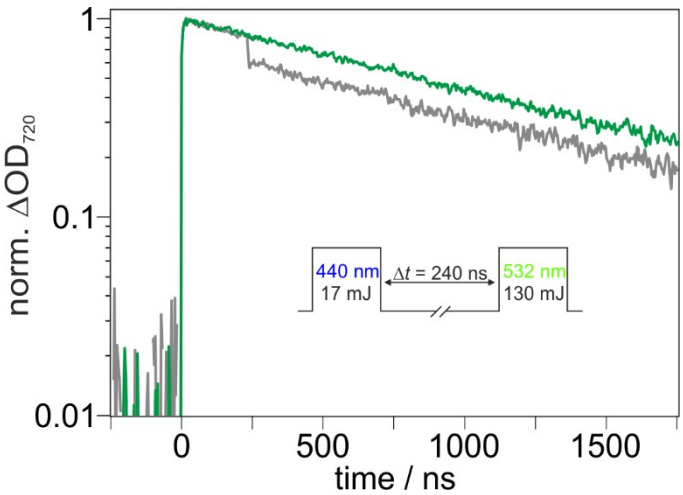

Fig. S6: Two-pulse experiment presented in Fig. 5a of the main paper with logarithmic y-axis to illustrate that the second pulse does not affect the kinetics for thermal charge recombination.

Two-pulse experiments on **TAA-ph$_2$-Ir-ph$_2$-AQ** are shown in Fig. S7. Transient absorption kinetics were detected at the spectral maximum of AQ$^{\bullet-}$ (panel a) and TAA$^{\bullet+}$ (panel b).

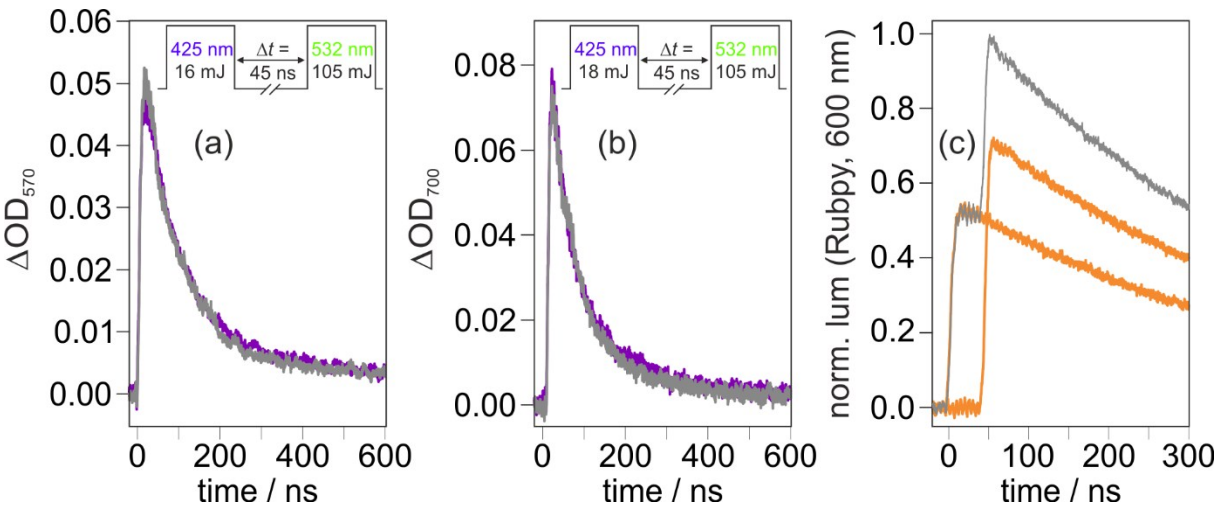

Fig. S7: Two-pulse experiments (pulse schemes are given above traces) on solutions of 40 µM **TAA-ph$_2$-Ir-ph$_2$-AQ** (panels a and b; in deoxygenated CH_3CN) and 10 µM $[Ru(bpy)_3]^{2+}$ (panel c, in air-saturated water). Kinetic traces for the triad were monitored at 570 nm (a) and 700 nm (b) with the second laser pulse blocked (violet) or unblocked (gray). The control experiments on the kinetic $[Ru(bpy)_3]^{2+}$ emission (panel c) serve to visualize the pulse scheme (same as in panel b). For details, see text.

The negligible second pulse induced absorption change during the experiments displayed in Fig. S7 (panels a and b) prompted us to visualize the pulse scheme with a control measurement on $[Ru(bpy)_3]^{2+}$ (panel c, very same laser settings as in panel b). The kinetic $[Ru(bpy)_3]^{2+}$ emission traces with just one laser (orange traces in panel c, the other pulse was selectively blocked) and both laser pulses (gray trace in Fig. S7c) clearly indicate that the desired pulse scheme has also been applied to **TAA-ph$_2$-Ir-ph$_2$-AQ**.
A comparative discussion of the two-pulse experiments on both triads is given in Section 2.4 of the main paper.

5 Supplementary references

1 S. Neumann and O. S. Wenger, *Inorg. Chem.*, 2019, **58**, 855–860.
2 M. Kuss-Petermann and O. S. Wenger, *Helv. Chim. Acta*, 2017, **100**, e1600283.
3 M. Montalti, A. Credi, L. Prodi and M. T. Gandolfi, *Handbook of photochemistry*, CRC/Taylor & Francis, Boca Raton, 3rd ed., 2006.
4 H. J. Kuhn, S. E. Braslavsky and R. Schmidt, *Pure Appl. Chem.*, 2004, **76**, 2105–2146.
5 S. Campagna, F. Puntoriero, F. Nastasi, G. Bergamini and V. Balzani, *Top. Curr. Chem.*, 2007, **280**, 117–214.
6 M. Goez, C. Kerzig and R. Naumann, *Angew. Chem. Int. Ed.*, 2014, **53**, 9914–9916.
7 P. Müller and K. Brettel, *Photochem. Photobiol. Sci.*, 2012, **11**, 632–636.
8 C. Kerzig and M. Goez, *Chem. Sci.*, 2016, **7**, 3862–3868.

9 C. Kerzig and O. S. Wenger, *Chem. Sci.*, 2018, **9**, 6670–6678.
10 C. Kerzig, X. Guo and O. S. Wenger, *J. Am. Chem. Soc.*, 2019, **141**, 2122–2127.
11 C. Kerzig and M. Goez, *Phys. Chem. Chem. Phys.*, 2014, **16**, 25342–25349.
12 M. Goez, D. von Ramin-Marro, M. H. Othman Musa and M. Schiewek, *J. Phys. Chem. A*, 2004, **108**, 1090–1100.
13 K. Sreenath, T. G. Thomas and K. R. Gopidas, *Org. Lett.*, 2011, **13**, 1134–1137.
14 R. F. Nelson and R. H. Philp, *J. Phys. Chem.*, 1979, **83**, 713–716.
15 J. L. Baptista and H. D. Burrows, *J. Chem. Soc. Faraday Trans. 1*, 1974, **70**, 2066–2079.
16 J. F. Ambrose, L. L. Carpenter and R. F. Nelson, *J. Electrochem. Soc.*, 1975, **122**, 876–894.
17 M. Büschel, C. Stadler, C. Lambert, M. Beck and J. Daub, *J. Electroanal. Chem.*, 2000, **484**, 24–32.
18 S. U. Pedersen, T. Bo Christensen, T. Thomasen and K. Daasbjerg, *J. Electroanal. Chem.*, 1998, **454**, 123–143.
19 A. Weller, *Z. Phys. Chem.*, 1982, **133**, 93–98.
20 L. G. Gagliardi, C. B. Castells, C. Ràfols, M. Rosés and E. Bosch, *J. Chem. Eng. Data*, 2007, **52**, 1103–1107.
21 M. J. Frisch, G. W. Trucks, H. B. Schlegel, G. E. Scuseria, M. A. Robb, J. R. Cheeseman, G. Scalmani, V. Barone, B. Mennucci, G. A. Petersson, H. Nakatsuji, M. Caricato, X. Li, H. P. Hratchian, A. F. Izmaylov, J. Bloino, G. Zheng, J. L. Sonnenberg, M. Hada, M. Ehara, K. Toyota, R. Fukuda, J. Hasegawa, M. Ishida, T. Nakajima, Y. Honda, O. Kitao, H. Nakai, T. Vreven, J. A. Montgomery, J. E. Peralta, F. Ogliaro, M. Bearpark, J. J. Heyd, E. Brothers, K. N. Kudin, V. N. Staroverov, R. Kobayashi, J. Normand, K. Raghavachari, A. Rendell, J. C. Burant, S. S. Iyengar, J. Tomasi, M. Cossi, N. Rega, J. M. Millam, M. Klene, J. E. Knox, J. B. Cross, V. Bakken, C. Adamo, J. Jaramillo, R. Gomperts, R. E. Stratmann, O. Yazyev, A. J. Austin, R. Cammi, C. Pomelli, J. W. Ochterski, R. L. Martin, K. Morokuma, V. G. Zakrzewski, G. A. Voth, P. Salvador, J. J. Dannenberg, S. Dapprich, A. D. Daniels, Farkas, J. B. Foresman, J. V. Ortiz, J. Cioslowski, and D. J. Fox. Gaussian 09 Revision B.01, 2010.
22 M. S. Lowry, J. I. Goldsmith, J. D. Slinker, R. Rohl, R. A. Pascal, G. G. Malliaras and S. Bernhard, *Chem. Mater.*, 2005, **17**, 5712–5719.
23 D. Hanss, J. C. Freys, G. Bernardinelli and O. S. Wenger, *Eur. J. Inorg. Chem.*, 2009, **2009**, 4850–4859.
24 C. K. Prier, D. A. Rankic and D. W. C. MacMillan, *Chem. Rev.*, 2013, **113**, 5322–5363.